Nonlinear damping in mechanical resonators made from carbon nanotubes and graphene

A. Eichler[1†], J. Moser[1†], J. Chaste[1], M. Zdrojek[1], I. Wilson-Rae[2] and A. Bachtold[1*]

The theory of damping is discussed in Newton's *Principia*[1] and has been tested in objects as diverse as the Foucault pendulum, the mirrors in gravitational-wave detectors and submicrometre mechanical resonators. In general, the damping observed in these systems can be described by a linear damping force. Advances in nanofabrication mean that it is now possible to explore damping in systems with one or more atomic-scale dimensions. Here we study the damping of mechanical resonators based on carbon nanotubes[2-11] and graphene sheets[12-15]. The damping is found to strongly depend on the amplitude of motion, and can be described by a nonlinear rather than a linear damping force. We exploit the nonlinear nature of damping in these systems to improve the figures of merit for both nanotube and graphene resonators. For instance, we achieve a quality factor of 100,000 for a graphene resonator.

Damping has an important impact on the dynamic behaviour of nanoelectromechanical systems (NEMS), and this influences the performance of NEMS-based devices in fundamental tests of quantum theory[16,17] and also in applications such as mass and force sensing[18,19]. So far it has always been possible to describe damping by a linear damping force $\gamma\, dx/dt$, where γ is the associated damping coefficient, x is the deflection of the resonator and t is time. Remarkably, this model can describe the damping of resonators with dimensions that range from the metre-scale down to a few tens of nanometres. In this work we study resonators with atomic-scale transverse dimensions, and show that the simple linear damping scenario breaks down and that the behaviour of nanotube and graphene resonators can instead be explained by a nonlinear damping force $\eta x^2\, dx/dt$, where η is the coefficient of nonlinear damping. We also demonstrate that the quality factor strongly varies with the driving force[12] and analyse this behaviour in light of the nonlinear damping theory[20].

We perform measurements on graphene and nanotube resonators (Fig. 1a,b) at low temperature and in high vacuum, using a dilution refrigerator with a base temperature of 90 mK. The resonator is actuated electrostatically by applying an oscillating voltage with an amplitude V^{AC} at frequency f between the resonator and a gate electrode (Fig. 1c). The motion is detected using the frequency-modulation mixing technique, where the resonator acts as a frequency mixer to deliver a mixing current $I_{mix} \propto \left| \partial \mathrm{Re}[x_0]/\partial f \right|$ (with $\mathrm{Re}[x_0]$ the real part of the motional amplitude x_0)[10]. The mixing current as a function of driving frequency f has a characteristic resonance lineshape that allows us to extract the mechanical quality factor Q in a simple manner (Fig. 1d): the resonance peak at frequency f_0 is flanked by two minima whose separation is the resonance width $\Delta f = f_0/Q$ for a linear harmonic oscillator. This simple relation is expected to break down in the presence of nonlinearities (see Fig. 1e), but an analogous expression is recovered in the limit of strong nonlinear damping, as discussed below (and in Supplementary Section D).

To show that nonlinear damping in graphene and nanotube NEMS is a robust phenomenon, we study three types of mechanical resonators: (1) a nanotube under tensile stress, (2) a nanotube with slack and (3) a graphene sheet under tensile stress. We estimate the built-in stress in each of these devices by measuring their basic mechanical properties. As an example, Fig. 2a shows the dependence of the resonance frequency on gate voltage V_g^{DC} for a nanotube resonator. The convex parabola has an electrostatic origin[21,22] and indicates that the nanotube is under tensile stress (schematic diagram of Fig. 2a)[14,15].

Figure 2b shows the resonant response of the stressed nanotube resonator for three different driving forces (which scale linearly with V^{AC}). As we increase the driving force, the resonance frequency shifts towards higher values and, simultaneously, the resonance peak broadens (see the bars below the resonances). Both these effects are also seen in Fig. 2c,d. In these measurements, care is taken to avoid driving V^{AC} above $k_B T/e$ in order to prevent electronic nonlinear effects or local heating (here k_B is the Boltzmann constant, T the temperature and e the electron charge). Although resonance shift is a known phenomenon (see below), resonance broadening is a new one. In larger resonators, resonance width is indeed independent of driving force ($\Delta f = f_0/Q = \gamma/2\pi m$, where m is the mass of the resonator).
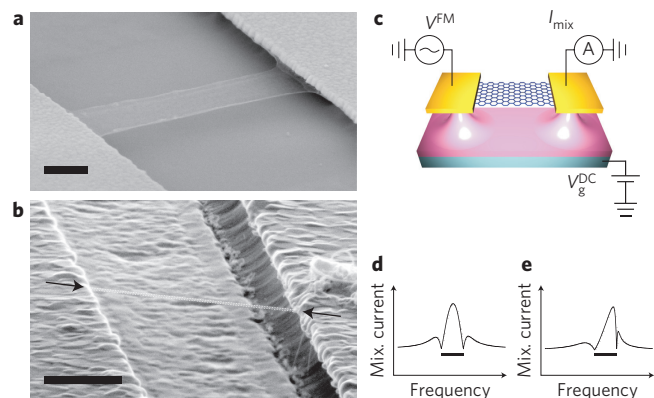
Figure 1 | Devices and measurement setup. a, Scanning electron micrograph of a suspended single-layer graphene sheet with Au contacts. Scale bar, 500 nm. **b**, Scanning electron micrograph of a nanotube grown by chemical vapour deposition over a prefabricated trench between two W/Pt contacts. The nanotube is marked by black arrows and white dotted lines. Scale bar, 500 nm. **c**, Schematic of the actuation/detection setup. A frequency-modulated voltage $V^{FM} = V^{AC}\cos[2\pi f t + (f_\Delta/f_L)\sin(2\pi f_L t)]$ is applied to the device. The motion is detected by measuring the mixing current at f_L. **d,e**, Schematic of the frequency response of the mixing current. The separation between the two minima (black bar) corresponds to the resonance width Δf. The resonance peak becomes asymmetric in the presence of a Duffing nonlinearity (**e**).

[1]CIN2 (ICN-CSIC), Catalan Institute of Nanotechnology, Campus de la UAB 08193 Bellaterra, Barcelona, Spain; [2]Technische Universität München, 85748 Garching, Germany; [†]These authors contributed equally to this work. *e-mail: adrian.bachtold@cin2.es
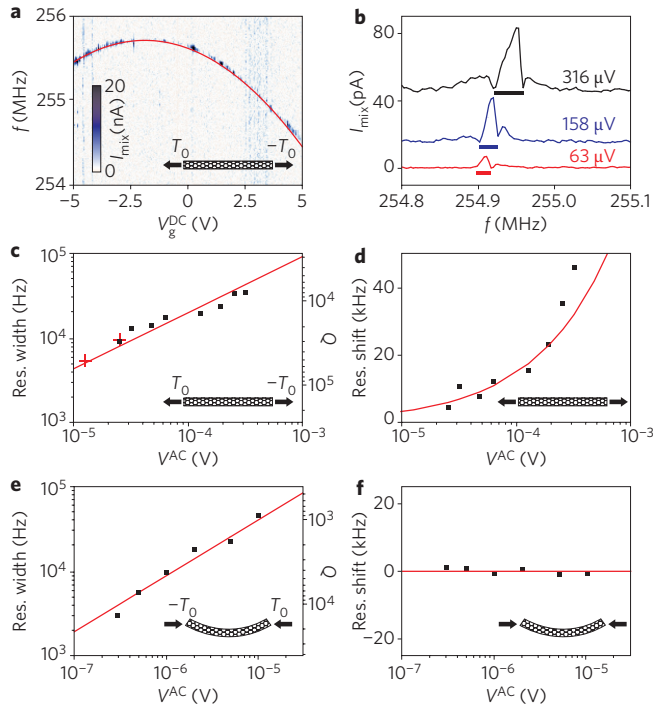
Figure 2 | Nonlinear damping in nanotube resonators. a, Resonance frequency as a function of gate voltage V_g^{DC} (by measuring I_{mix} as a function of f and V_g^{DC}) for a nanotube under tensile stress. The red line corresponds to a fit to a model based on electrostatic considerations (see Supplementary Information). The length of the nanotube is 840 nm and the radius is 2 nm. The device is fabricated by depositing the contact electrodes onto the nanotube. T_0 denotes the built-in tension of the resonator. The faint background is related to noise in I_{mix}. **b**, Frequency response of the mixing current for three different values of driving forces (or, equivalently, three different values of V^{AC}). Both the resonance width and the resonance frequency increase as the driving force increases. Curves are offset for clarity. **c**, Resonance width as a function of V^{AC}. Black squares correspond to 5 K and red crosses to 400 mK. The red line is a solution to equation (2) with $\eta = 10^4$ kg m^{-2} s^{-1} ($\gamma = 0$). Q is shown on the right-hand-side scale. **d**, Resonance shift as a function of V^{AC}. The red line is a solution to equation (1) with $\alpha = 6 \times 10^{12}$ kg m^{-2} s^{-2}. **e**, Resonance width as a function of V^{AC} for a nanotube with slack at 100 mK. The red line is a solution to equation (2) with $\eta = 7.9 \times 10^5$ kg m^{-2} s^{-1} ($\gamma = 0$). **f**, Resonance shift as a function of V^{AC}. The red line is a solution to equation (1) with $\alpha \leq 4.8 \times 10^{12}$ kg m^{-2} s^{-2} (the upper limit of α is obtained from measurement uncertainties). The length of the nanotube is 2 μm and the radius is 1.5 nm. The device is fabricated by growing the tube over the predefined electrodes.

The same measurement is performed on the nanotube with slack (schematic of Fig. 2e) and on the graphene sheet under tensile stress (schematic of Fig. 3a). Resonance broadening is observed in all three types of resonators (Figs 2c,e and 3a) and even at room temperature (Supplementary Fig. S10). This confirms that the effect is robust, and is also consistent with the results of early optical measurements on graphene[12]. The resonance broadening does not stem from the coupling between electrons and mechanical vibrations[8,9] because the effect is not associated with Coulomb blockade and V^{AC} is kept below $k_B T/e$ (for more discussions see Supplementary Section J). The resonance shift shows different behaviour: it is significant for resonators under tensile stress (Figs 2d and 3b), but is negligible (Fig. 2f) and sometimes even negative (Supplementary Fig. S10) for nanotube resonators with slack. Further discussion, as well as
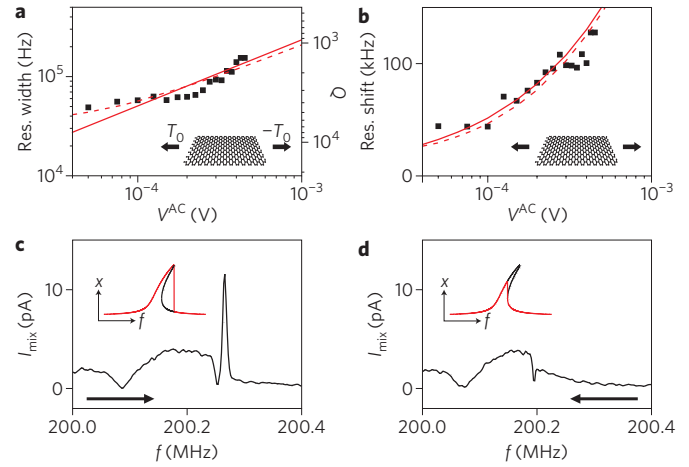
Figure 3 | Nonlinear damping in a graphene resonator. a,b, Resonance width and quality factor (**a**) and resonance shift (**b**) as a function of V^{AC} for a graphene sheet under tensile stress at 4 K. The solid red lines are obtained with $\eta = 2.4 \times 10^7$ kg m^{-2} s^{-1} and $\alpha = 1.9 \times 10^{16}$ kg m^{-2} s^{-2} ($\gamma = 0$). The dashed red lines represent an improved fit with finite linear damping ($\eta = 1.5 \times 10^7$ kg m^{-2} s^{-1}, $\alpha = 1.4 \times 10^{16}$ kg m^{-2} s^{-2}, $\gamma = 8.7 \times 10^{-14}$ kg s^{-1}). The length of the graphene is 1.7 μm and the width is 120 nm. **c,d**, Frequency response of the mixing current at $V^{AC} = 0.5$ mV as the frequency is swept upwards (**c**) and downwards (**d**). Insets: schematics showing the amplitude of motion as a function of driving frequency (red curves) and the solutions of equation (1) (black curves).

additional electrical and mechanical characterizations, can be found in Supplementary Sections E–G.

On further increasing V^{AC}, we observe a hysteretic response for the graphene resonator but not for any of the two nanotube resonators. In the case of the graphene resonator, the resonance lineshape differs, depending on whether the driving frequency is swept upwards or downwards (Fig. 3c,d). The hysteresis is intimately related to the resonance shift[22–24]. They both originate from the so-called Duffing force αx^3 (ref. 20). The latter contributes to the restoring force, which makes the resonator stiffer (for $\alpha > 0$) and increases the resonance frequency. For sufficiently large driving forces, the motional amplitude as a function of driving frequency f develops an asymmetry (black curve in the schematic of Fig. 3c). This results in bistability and hysteresis for certain intervals in f (red curves in the schematics of Fig. 3c,d). In this context, the absence of hysteresis in some of our devices is intriguing.

We now show that the broadening of resonance and the occasional absence of hysteresis that we observe can be understood within a nonlinear framework. In addition to the Duffing nonlinearity αx^3, the other relevant higher-order term in the Newton equation for a harmonic oscillator is the nonlinear damping term $\eta x^2 \, dx/dt$ (refs 20,25):

$$m\,d^2x/dt^2 = -kx - \gamma dx/dt - \alpha x^3 - \eta x^2 dx/dt \\ + F_{drive}\cos(2\pi ft) \qquad (1)$$

Here F_{drive} is the driving force amplitude and k the spring constant. Equation (1) provides a general treatment of nonlinear resonators, in the sense that, in the limit of weak damping and weak anharmonicity, additional terms of second and third order (x^2, xdx/dt, $(dx/dt)^2$, $x(dx/dt)^2$, $(dx/dt)^3$) merely lead to a renormalization of α and η (ref. 20). A derivation of equation (1) based on a nonlinear Caldeira–Leggett model can be found in ref. 25, in which the nonlinear damping force emerges from the interaction of the mechanical resonator with a thermal bath of harmonic degrees of freedom.

Dissipation is described by the terms $\gamma\, dx/dt$ and $\eta x^2\, dx/dt$. The latter term is special because it accounts for a dissipation mechanism that becomes important at large motional amplitude. When $\gamma\, dx/dt$ is dominant over $\eta x^2\, dx/dt$, which is the case for larger mechanical resonators, resonance width is independent of driving force and is given by $\Delta f = \gamma/2\pi m$. In the other limit, when the $\gamma\, dx/dt$ term can be neglected, we obtain (Supplementary Section D)

$$\Delta f = 0.032 m^{-1}\eta^{1/3}f_0^{-2/3}F_{\text{drive}}^{2/3} \qquad (2)$$

so that $\Delta f \propto (V^{\text{AC}})^{2/3}$. This dependence is in good agreement with the experimental data (red lines in Figs 2c,e and 3a) and is used to extract η (Δf tends to saturate at low V^{AC} for some devices, which may signal that linear damping begins to play a role; see Fig. 3a). The shift of the resonance frequency as a function of V^{AC} is determined from the maximum of I_{mix} and is then compared with the steady-state solution of equation (1) using α as fit parameter (see Supplementary Section H). Agreement between theory and experiment is satisfactory (red line in Figs 2d,f and 3b).

The occasional absence of hysteresis is a direct consequence of nonlinear damping and can be predicted from the ratio between α and η. When $\eta/\alpha > \sqrt{3}/2\pi f_0$, the nonlinear damping is strong enough to keep the broadening of resonance always comparable to or larger than its shift and precludes hysteresis for all driving forces[20]. Using the values of α and η obtained from the aforementioned fitting, we find that η/α is larger than $\sqrt{3}/2\pi f_0$ for the two nanotube resonators in Fig. 2. Thus no hysteresis is expected, in agreement with the experiment. In contrast, we obtain $\eta/\alpha < \sqrt{3}/2\pi f_0$ for the graphene resonator in Fig. 3 and the predicted hysteresis is indeed observed.

The physical origin of nonlinear damping is a subtle problem that has thus far been underappreciated. A possible explanation is that it stems from the concerted effect of (1) a standard dissipation channel, which alone would lead to purely linear damping (such as contamination), and (2) geometrical nonlinearity, which can arise from the elongation of a doubly clamped resonator on deflection (see Supplementary Section E for experimental evidence of the geometrical nonlinearity effect). Such a scenario has been analysed for a dissipation mechanism described by a phenomenological viscoelastic model[25], yielding the relation $\eta = 4\gamma/r^2$ for a rod under tensile stress. This leads to $\eta < 260\ \text{kg m}^{-2}\ \text{s}^{-1}$ from Fig. 2c (where we can estimate an upper bound for γ using $2\pi m\,\min(\Delta f) = 2.5 \times 10^{-16}\ \text{kg s}^{-1}$). This does not compare well with the value obtained from the fit ($\eta = 1 \times 10^4\ \text{kg m}^{-2}\ \text{s}^{-1}$), which suggests that the underlying physics is different. The viscoelastic model assumes that the dissipation is internal to the resonator, so the observed nonlinear damping could be associated with a dissipation channel exterior to the resonator, such as clamping losses (phonon tunnelling[26]). Alternatively, geometric nonlinearity may not play any role and the nonlinearity of the damping may be germane to the dissipation mechanism itself, for example, friction associated with the sliding between the nanotube/graphene and the metal electrode. Another possible contribution could stem from the nonlinearities in phonon–phonon interactions. However, theoretical analyses of nonlinear damping are scarce, possibly because it has not seemed relevant, and more theoretical work is required. On the experimental side, there is a need to study the dependence of nonlinear damping force on contamination, clamping configuration and suspended length.

One may wonder whether the relationship between Δf and Q remains meaningful when the damping is strongly nonlinear. Provided that Δf and the resonance shift are much smaller than f_0, the standard definition of Q in terms of the free-ringdown is still warranted and reads $Q = 2\pi E/\Delta E$, where ΔE is the mechanical energy lost over one oscillation period and E is the corresponding
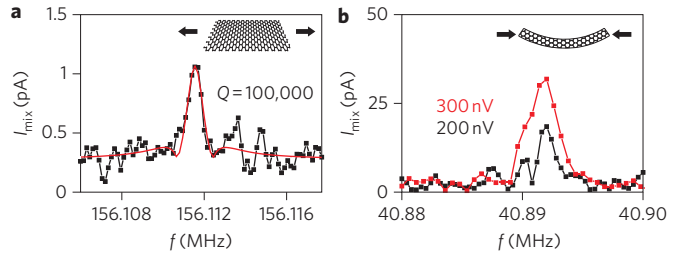
Figure 4 | Quality factor and force sensitivity at low driving force. a, Mixing current versus frequency for a graphene resonator under tensile stress at 90 mK ($V^{\text{AC}} = 8\ \mu\text{V}$) showing an ultrahigh quality factor (100,000). The red curve is a fit. The length of the graphene is 2 μm and the width is 800 nm. Additional resonance curves are shown in Supplementary Fig. S5. **b**, Mixing current versus frequency for a nanotube with slack for two values of V^{AC} at 100 mK showing an ultralow force sensitivity (2.5 aN Hz$^{-1/2}$). This is the same sample as in Fig. 2.

time-averaged stored energy. Moreover, equation (1) yields a quality factor that depends on $|x_0|$, the modulus of the slowly decaying free oscillation amplitude, and is given by $Q = 8\pi f_0 m/\eta|x_0|^{-2}$ when γ is neglected. To make the connection with a driven resonator, we take $|x_0|$ as the maximum amplitude of the response and find that Q satisfies

$$Q = 1.09 f_0/\Delta f \qquad (3)$$

(Supplementary Section D). This simple relation is all the more surprising because it is very close to that of a simple harmonic oscillator.

The ability to vary the resonance width allows us to improve the mechanical quality factor. To achieve larger Q-factors, we simply lower the driving force until the motion becomes barely detectable. For this, it is convenient to select the value of V_g^{DC} for which the detection signal is largest. In so doing, we measure a quality factor of 100,000 for a graphene resonator at 90 mK (Fig. 4a). This is the largest Q ever reported in a graphene resonator.

Larger quality factors enable better force sensing. Figure 4b shows the resonances of a nanotube at very low driving forces (with V^{AC} as low as 200 nV). Using $C' = -5.2 \times 10^{-12}\ \text{F m}^{-1}$ (Supplementary Section E), $V_g^{\text{DC}} = 2.49\ \text{V}$ and the 1 Hz measurement bandwidth, we obtain a force sensitivity of 2.5 aN Hz$^{-1/2}$ (here the force is $C'V_g^{\text{DC}}V^{\text{AC}}$, where C' is the derivative of the gate-resonator capacitance with respect to x). This is within a factor of five of the best sensitivities reported using microfabricated resonators operating at their ultimate limit set by thermal vibrations[27,28]. As there is room to optimize the detection scheme, the sensitivity of nanotube/graphene resonators can in principle be further enhanced.

In conclusion, the fact that we have observed nonlinear damping in two distinct systems (nanotube and graphene resonators), and also under different conditions (both tensile stress and slack), means that many predictions will have to be revisited when they are applied to nanotube and graphene resonators, because these predictions assume linear damping (see, for example, refs 16–19). Moreover, nonlinear damping makes it possible to tune the quality factor of these resonators, which could prove useful in both fundamental research and applications.

Methods

We used three different strategies to fabricate our resonators. In one approach, we grew nanotubes by chemical vapour deposition on an oxidized silicon wafer. Nanotubes were contacted to metal electrodes by electron-beam lithography and were suspended in a wet etching step. In the second approach, we grew the nanotube in the last fabrication step over a predefined trench separating two electrodes[9]. Finally, we fabricated graphene resonators by depositing a single graphene layer onto an oxidized silicon wafer using the adhesive tape technique[29]. We contacted the

graphene sheet to metal electrodes and suspended it by etching the silicon oxide[30]. For further information see Supplementary Information.

References

1. Newton, I., *Principia, Book II* (1687).
2. Sazonova, V. *et al.* Tunable carbon nanotube electromechanical oscillator. *Nature* **431,** 284–287 (2004).
3. Garcia-Sanchez, D. *et al.* Mechanical detection of carbon nanotube resonator vibrations. *Phys. Rev. Lett.* **99,** 085501 (2007).
4. Lassagne, B., Garcia-Sanchez, D., Aguasca, A. & Bachtold, A. Ultrasensitive mass sensing with a nanotube electromechanical resonator. *Nano Lett.* **8,** 3735–3738 (2008).
5. Chiu, H-Y., Hung, P., Postma, H. W. Ch. & Bockrath, M. Atomic-scale mass sensing using carbon nanotube resonators. *Nano Letters* **8,** 4342–4346 (2008).
6. Jensen, K., Kim, K. & Zettl, A. An atomic-resolution nanomechanical mass sensor. *Nature Nanotech.* **3,** 533–537 (2008).
7. Hüttel, A. K. *et al.* Carbon nanotubes as ultrahigh quality factor mechanical resonators. *Nano Lett.* **9,** 2547–2552 (2009).
8. Lassagne, B, Tarakanov, Y., Kinaret, J., Garcia-Sanchez, D. & Bachtold, A. Coupling mechanics to charge transport in carbon nanotube mechanical resonators. *Science* **325,** 1107–1110 (2009).
9. Steele, G. A. *et al.* Strong coupling between single-electron tunneling and nanomechanical motion. *Science* **325,** 1103–1107 (2009).
10. Gouttenoire, V. *et al.* Digital and FM demodulation of a doubly clamped single-walled carbon-nanotube oscillator: towards a nanotube cell phone. *Small* **6,** 1060–1065 (2010).
11. Wang, Z. *et al.* Phase transitions of adsorbed atoms on the surface of a carbon nanotube. *Science* **327,** 552–555 (2010).
12. Bunch, J. S. *et al.* Electromechanical resonators from graphene sheets. *Science* **315,** 490–493 (2007).
13. Garcia-Sanchez, D. *et al.* Imaging mechanical vibrations in suspended graphene sheets. *Nano Lett.* **8,** 1399–1403 (2008).
14. Chen, C. *et al.* Performance of monolayer graphene nanomechanical resonators with electrical readout. *Nature Nanotech.* **4,** 861–867 (2009).
15. Singh, V. *et al.* Probing thermal expansion of graphene and modal dispersion at low-temperature using graphene nanoelectromechanical systems resonators. *Nanotechnology* **21,** 165204 (2010).
16. Katz, I., Retzker, A., Straub, R. & Lifshitz, R. Signatures for a classical to quantum transition of a driven nonlinear nanomechanical resonator. *Phys. Rev. Lett.* **99,** 040404 (2007).
17. Kippenberg, T. J. & Vahala, K. J. Cavity optomechanics: back-action at the mesoscale. *Science* **321,** 1172–1176 (2008).
18. Ekinci, K. L., Yang, Y. T. & Roukes, M. L. Ultimate limits of inertial mass sensing based upon nanoelectromechanical systems. *J. Appl. Phys.* **95,** 2682–2689 (2004).
19. Cleland, A. N. & Roukes, M. L. Noise processes in nanomechanical resonators. *J. Appl. Phys.* **92,** 2758–2769 (2002).
20. Lifshitz, R. & Cross, M. C. *Reviews of Nonlinear Dynamics and Complexity* Vol. 1 (Wiley-VCH, 2008), available at www.tau.ac.il/~ronlif/pubs/RNDC1-1-2008-preprint.pdf
21. Howe, R. T. & Muller, R. S. Resonant-microbridge vapor sensor. *IEEE Trans. Electron Devices* **ED-33,** 499–506 (1986).
22. Kozinsky, I., Postma, H. W. C., Bargatin, I. & Roukes, M. L. Tuning nonlinearity, dynamic range, and frequency of nanomechanical resonators. *Appl. Phys. Lett.* **88,** 253101 (2006).
23. Aldridge, J. S. & Cleland, A. N. Noise-enabled precision measurements of a Duffing nanomechanical resonator. *Phys. Rev. Lett.* **94,** 156403 (2005).
24. Unterreithmeier, Q. P., Faust, T. & Kotthaus, J. P. Nonlinear switching dynamics in a nanomechanical resonator. *Phys. Rev. B* **81,** 241405R (2010).
25. Zaitsev, S., Shtempluck, O., Buks, E. & Gottlieb, O. Nonlinear damping in a micromechanical oscillator. Preprint at http://arXiv.org/abs/0911.0833v2 (2009).
26. Wilson-Rae, I. Intrinsic dissipation in nanomechanical resonators due to phonon tunnelling. *Phys. Rev. B* **77,** 245418 (2008).
27. Mamin, H. J. & Rugar, D. Sub-attonewton force detection at millikelvin temperatures. *Appl. Phys. Lett.* **79,** 3358 (2001).
28. Teufel, J. D., Donner, T., Castellanos-Beltran, M. A., Harlow, J. W. & Lehnert, K. W. Nanomechanical motion measured with an imprecision below that at the standard quantum limit. *Nature Nanotech.* **4,** 820–823 (2009).
29. Novoselov, K. S. *et al.* Two-dimensional atomic crystals. *Proc. Natl Acad. Sci. USA* **102,** 10451–10453 (2005).
30. Moser, J. & Bachtold, A. Fabrication of large addition energy quantum dots in graphene. *Appl. Phys. Lett.* **95,** 173506 (2009).

Acknowledgements

Author contributions

A.E., J.M. and M.Z. fabricated the devices. J.M. and A.E. developed the measurement setup and performed the measurements. J.C. and A.B. provided measurement support. A.E., J.M., A.B. and I.W.-R. analysed the data. I.W.-R. established equations (2) and (3). A.B. conceived and designed the experiment. All authors contributed to writing the manuscript.

Additional information